

## INDUCED COMPTON BACKSCATTERING IN RADIO PULSARS AND RADIO-LOUD ACTIVE GALACTIC NUCLEI

MARK W. SINCELL

Department of Physics MC 704, University of Illinois at Urbana-Champaign, 1110 W. Green Street, Urbana, IL 61801-3080

AND

PAOLO S. COPPI

Department of Astronomy, Yale University, P.O. Box 208101, New Haven, CT 06520-8101

Received 1995 May 1; accepted 1995 September 26

### ABSTRACT

We perform a quantitative numerical calculation of the steady-state radiation spectrum in a slab of cold electrons which is illuminated by unpolarized collimated, high brightness temperature radiation. The process of induced Compton backscattering can dramatically increase the intensity of radiation reflected from the slab over the level predicted by spontaneous scattering when the incident radiation spectrum has a spectral index  $\alpha > 1$  (where the flux density  $S_\nu \propto \nu^\alpha$ ). In this case, the reflected spectrum has a spectral index  $\alpha \geq 1$  up to a cutoff at the peak frequency ( $\nu_0$ ) of the illuminating radiation spectrum. When the incident spectrum has a spectral index  $\alpha < 1$ , the intensity of the reflected radiation is instead strongly reduced and a broad absorption-like feature appears in the reflected spectrum at  $\nu \gtrsim \nu_0$ . In agreement with previous order of magnitude estimates, we find that induced Compton backscattering limits the brightness temperature at the peak of the transmitted flux density spectrum to  $(kT_B/m_e c^2)\tau_T^2 \theta^2 = 1.0$ , where  $\theta$  is the opening angle of the beam and  $\tau_T$  is the Thomson depth of the slab. The polarization of the backscattered flux can be exponentially magnified if the incident radiation has a small net polarization. Induced Compton backscattering also rapidly transfers momentum from the incident radiation beam to the scattering electrons and can significantly enhance the radiation pressure force on the illuminated side of the scattering plasma.

Applying these results to a simple spherically symmetric model of a magnetized pulsar wind, we find that the pulsed emission from radio pulsars with  $P \lesssim 0.1 \dot{P}_{-15}^{1/5}$  s should be obscured by stimulated backscattering. We argue that the electron density along the path of the radio emission must be substantially underdense relative to the predictions of the simplest wind model, perhaps as the result of a large induced radiation pressure force. Stimulated backscattering enhances the reflected flux density from the parsec scale material in the centers of radio-loud active galactic nuclei, and the flux from the reflection nebulae could be as much as a few percent of the total observed flux. The reflected flux density is characterized by  $S_\nu \propto \nu$  and strong frequency-dependent polarization.

*Subject headings:* galaxies: active — pulsars: general — radiative transfer — radio continuum: galaxies

### 1. INTRODUCTION

Very high brightness temperature ( $T_b$ ) radio emission is either observed or inferred in pulsars and radio-loud active galactic nuclei (AGNs) (Lyne & Graham-Smith 1990; Kellerman & Pauliny-Tóth 1981). The exceptionally large photon occupation numbers that are implied by these brightness temperatures suggest that stimulated scattering processes could play an important role in determining the character of the emission from these objects. However, as Kompaneets (1957) observed, recoilless stimulated scattering has no net effect upon a photon distribution and the small magnitude of the electron recoil when radio photons are scattered means that the effects of stimulated (induced) Compton scattering become important relative to those of ordinary (spontaneous) Thomson scattering only when  $(kT_B/m_e c^2)\tau_T \gtrsim 1$ . Nevertheless, the brightness temperatures in radio-loud AGNs and pulsars are orders of magnitude greater than  $m_e c^2/k = 5 \times 10^9$  K and stimulated scattering may indeed be an important process in these objects (Coppi, Blandford, & Rees 1993, hereafter CBR93; Sincell & Krolik 1994).

The general theory of induced Compton scattering is well developed (Weymann 1965; Peyraud 1968a, b, c) and the implications of the general theory have been explored in a

variety of astrophysical situations (Zel'dovich & Sunyaev 1969; Sunyaev 1971; Zel'dovich & Levich 1975; Montes 1977; Sincell & Krolik 1992, hereafter SK92; CBR93; Thompson et al. 1994; Sincell & Krolik 1994). The stimulated scattering of photons causes them to move monotonically downward in energy and results in a net transfer of energy to the scattering electrons. The observed flux density from a source embedded in a plasma of Thomson depth  $\tau_T$  peak at the highest frequency for which the induced scattering optical depth  $\tau_i \simeq (kT_B/m_e c^2)\tau_T \simeq 1$ . Below this frequency, the flux density is given by the equilibrium distribution  $S_\nu \propto \nu$  (Wilson 1982; CBR93). The increased scattering rate can greatly enhance the radiation force on the electrons (Levich 1972).

The stimulated scattering rate is strongly dependent upon the angular distribution of the high brightness temperature radiation (Gol'din, Sunyaev, & Chetverushkin 1975; Zel'dovich & Sunyaev 1976; Wilson & Rees 1978; SK92). Collimation of the photon distribution into a beam of opening angle  $\theta \ll 1$ , either by the emission process or simple radial streaming away from the source, reduces the stimulated scattering rate by  $\theta^4$ . Two factors of  $\theta$  arise in the integration over the beam solid angle, and two more come from the fact that the maximum electron recoil energy is

$\propto(1 - \cos \theta) \propto \theta^2$ . As noted in CBR93, however, this estimate depends critically on the assumption that there are no photons outside the beam so that induced scattering rate into directions outside the beam is zero. This is not likely to be true in practice. In particular, once the radiation beam enters a scattering medium, spontaneous scattering will begin to isotropize the beam. If the beam travels through a Thomson scattering optical depth  $\tau_T \gtrsim \theta^2$ , the radiation field formed by the spontaneous scattering of beam photons is sufficiently intense that induced Compton scattering of beam photons into directions outside the beam actually dominates over induced scattering within the beam. Significant distortions in the beam spectrum are expected if  $(kT_B/m_e c^2)\tau_T^2 \theta^2 \gtrsim 1$  (Thompson et al. 1994). In other words, the effects of stimulated scattering on a beam can be significantly enhanced when the presence of spontaneously scattered radiation is taken into account. We will refer to the process by which this occurs as induced Compton backscattering since the coupling of the beam radiation to the spontaneously scattered radiation turns out to be strongest in the backscattering ( $\theta = \pi$ ) direction.

Most previous studies of the effects of induced Compton scattering on the spectrum and angular distribution of highly collimated high brightness temperature radiation (Gol'din et al. 1975; Wilson & Rees 1978; SK92) make the simplifying assumption that the photon occupation number outside of the beam is zero. Thus they do not consider stimulated backscattering. Recognizing the possible importance of stimulated backscattering in eclipsing millisecond binary pulsars, Thompson et al. (1994) made order of magnitude estimates of the stimulated backscattering optical depth of a scattering slab. CBR93 present a numerical simulation of the evolution of the spectrum and angular distribution of a high brightness temperature photon beam with an opening angle of  $\Delta\Omega = \pi/3$ . In this work, we expand upon CBR93 and present a quantitative calculation of the steady-state radiation field in a scattering slab as a function of  $\tau_T$ ,  $\theta$ , and the brightness temperature of the illuminating radiation. The goal of this study is to define when stimulated backscattering is an important process, what the observable consequences are, and to outline possible implications for radio pulsars and radio loud AGNs.

The nonlinear nature of induced Compton backscattering precludes a complete analytic treatment of the process, so we concentrate most of our effort on a numerical simulation. However, some insight into the qualitative features of induced Compton backscattering can be found using a simple analytic model of the process, which we present in § 2. The numerical method is presented in § 3 and the results are discussed in § 4. The application of this model to pulsars and radio-loud AGNs is discussed in § 5 and we conclude in § 6.

## 2. INDUCED COMPTON BACKSCATTERING

The kinetic equation which describes the transfer of radiation through a cold electron plasma is

$$\frac{\partial y_1}{\partial t} + c(\mathbf{\Omega}_1 \cdot \nabla)y_1 = -n_e(x)\sigma_T c y_1 + \frac{3n_e(x)\sigma_T c}{16\pi} \times \int d\Omega_2 [1 + (\mathbf{\Omega}_1 \cdot \mathbf{\Omega}_2)^2] \left[ y_2 + 2y_1 \frac{\partial y_2}{\partial v} (1 - \mathbf{\Omega}_1 \cdot \mathbf{\Omega}_2) \right], \quad (1)$$

where  $y_i = y(\mathbf{\Omega}_i, \mathbf{x}, \nu, t)$ ,  $\mathbf{\Omega}_{1,2}$  are the unit vectors in the direction of photon propagation,  $\nu$  is the photon frequency,  $n_e(\mathbf{x})$  is the local electron density, and  $(\mathbf{x}, t)$  are the time and space coordinates in the scattering plasma. Here we have introduced the variable

$$y = \frac{\eta h \nu^2}{m_e c^2} = \frac{kT_B \nu}{m_e c^2} = \frac{I_\nu}{2m_e \nu}, \quad (2)$$

where  $\eta$  is the photon occupation number and  $I_\nu$  is the spectral intensity (Wilson & Rees 1978). The variable  $y$  has dimensions of frequency.

The qualitative features of the steady state radiation spectrum in a geometrically and optically thin slab which is illuminated by collimated radiation can be described by a simple pair of equations. First, we assume that the radiation field can be divided into a highly collimated primary component with a constant value  $y_p$  throughout the angle  $\theta \ll 1$  and an isotropic secondary component,  $y_s$ . If one assumes that  $y_s \ll y_p$  (equivalent to assuming that  $\tau_T \ll 1$ ), then equation (1) reduces to a pair of equations describing the evolution of the two components of the radiation field

$$\frac{\partial y_p}{\partial \tau} = -y_p + 2y_p \frac{\partial y_s}{\partial \nu} + 3f^2 y_p \frac{\partial y_p}{\partial \nu}, \quad (3)$$

$$\frac{\partial y_s}{\partial \tau} = -f y_p - 2f y_s \frac{\partial y_p}{\partial \nu}, \quad (4)$$

where  $4\pi f \simeq \pi\theta^2$  is the solid angle subtended by the primary beam. Equation (3) is derived by assuming that  $\mathbf{\Omega}_1$  is parallel to the beam direction, and equation (4) is derived assuming that  $\mathbf{\Omega}_1$  is antiparallel to the beam. In these equations we have neglected spontaneous scattering from the secondary back to the primary and terms which are quadratic in  $y_s$ . These approximations will not necessarily be satisfied in the simulations, where we use the full kinetic equations and follow the nonlinear growth of the secondary, but they do apply in the early stages of the beam evolution. We note that CBR93 obtained a similar set of equations. The second term on the right-hand side of each of these two equations describes the coupling of the isotropic component to the beamed radiation, and therefore describes stimulated backscattering. The third term on the right-hand side of equation (3) describes the effects of stimulated scattering events which couple different photon states *within* the beam. We will refer to this process as “in-beam” scattering (CBR93 use the term “self-induced”).

Stimulated backscattering will control the evolution of the primary and secondary components of the radiation field for a wide range of parameters. First, if we neglect the effects of stimulated scattering on the secondary, then the spontaneously scattered radiation field at a Thomson depth  $\tau$  from the inner edge of a slab of total depth  $\tau_T$  is

$$y_s(\tau) \simeq f(\tau_T - \tau)y_p. \quad (5)$$

Comparing terms in equations (3) and (4) and using equation (5) to estimate  $y_s$ , we find that the stimulated backscattering rate exceeds the Thomson scattering rate at the inner edge of the slab ( $\tau = 0$ ) when

$$\frac{kT_B}{m_e c^2} \gtrsim \frac{1}{2f\tau_T}. \quad (6)$$

Second, the stimulated backscattering rate for photons in

the beam (i.e., the primary component) exceeds the in-beam scattering rate when

$$\tau_T \gtrsim \frac{3}{2} f. \quad (7)$$

The conditions (6) and (7) define the range of parameters for which stimulated backscattering determines the steady state spectrum of the beam.

The qualitative effect of stimulated backscattering on the spectra of the primary and secondary radiation fields can also be illustrated using equations (3) and (4). Under the assumptions (6) and (7), the steady state photon distribution can be described by a deceptively simple pair of equations

$$\frac{\partial y_p}{\partial \tau} = 2y_p \frac{\partial y_s}{\partial v}, \quad (8)$$

$$\frac{\partial y_s}{\partial \tau} = -2fy_s \frac{\partial y_p}{\partial v}. \quad (9)$$

We define a quantity called the backscatter optical depth as

$$\tau_{BS}(v) = \frac{kT_B(v)}{m_e c^2} \tau_T^2 \theta^2 \sim \frac{\Delta y_p}{y_p}, \quad (10)$$

and we expect induced Compton scattering to significantly change the intensity of the beamed radiation at frequencies where  $\tau_{BS}(v) \gtrsim 1$ . For  $\tau_T$  sufficiently small that  $\tau_{BS}(v) \lesssim 1$ , the intensity in the primary remains approximately constant while the secondary evolves on a dimensionless  $e$ -folding scale of  $\tau \simeq m_e c^2 / f k T_B$ . When  $\partial y_p / \partial v > 0$ , increasing  $\tau_T$  causes the intensity of the secondary at the inner edge of the slab to grow exponentially and when  $\partial y_p / \partial v < 0$  the intensity decreases. When  $\tau_{BS}$  reaches a certain limiting value (see § 4.2 for the exact value as determined by our simulations), the feedback of the secondary on the primary must be taken into account and the exponential growth of the secondary saturates. Determining the slab radiation spectrum in this case is nontrivial and is the subject of the next two sections.

### 3. NUMERICAL METHOD

Equation (1) is integrated numerically by calculating the local evolution of the radiation field caused by scattering and then transporting the photons between nearest neighbors in a face-centered cubic lattice. This method is described in detail by CBR93, so we limit ourselves to a short discussion. The radiation field at each point in the lattice is divided into solid angle bins and logarithmic frequency bins. Stimulated scattering causes the variable  $\tilde{y}$  to evolve according to

$$\frac{\partial \tilde{y}_i(\tilde{v})}{\partial t_c} = \tilde{y}_i(\tilde{v}) \sum_j C_{ij} \frac{\partial \tilde{y}_j(\tilde{v})}{\partial \tilde{v}}, \quad (11)$$

where  $\tilde{y}$  and  $\tilde{v}$  are the dimensionless integration variables and  $t_c = n_e \sigma_T c t$  is the time in Thomson units. The weighting factor,  $C_{ij}$ , is calculated using the angular factors in equation (1) and is

$$C_{ij} = \frac{3}{16\pi} [1 + (\mathbf{\Omega}_i \cdot \mathbf{\Omega}_j)^2] (1 - \mathbf{\Omega}_i \cdot \mathbf{\Omega}_j) \Delta \Omega_i, \quad (12)$$

where  $\Delta \Omega_i$  is the solid angle subtended by angular bin  $i$ . Spontaneous scattering by the electrons is also included in the simulation.

There are two major differences between the model used in CBR93 and the one presented here. First, we use a different time step

$$\Delta t_c = \text{Min} \left[ \frac{\Delta \tilde{v}_k}{1.2 C_{ij} (\partial \tilde{y}_j / \partial \tilde{v}_k) + 1} \right], \quad (13)$$

where  $\Delta \tilde{v}_k$  is the width of the frequency bin,  $k$ . The minimum is taken over the initial solid angle bins, indicated by the subscript  $i$ , and the frequency bins,  $k$ . We find that this prescription maintains the stability of the model up to much larger values of  $\tilde{y}$ . Second, we have added eight solid angle bins to represent the beam. Each of these has a solid angle of  $\Delta \Omega \simeq \pi \theta^2 / 9$ , and photons in these bins propagate along the nearest neighbor direction corresponding to the beam direction, i.e., perpendicular to the slab.

The amplitude of the radiation antiparallel to the beam dominates the backscattered radiation field for  $\tau_T \lesssim 0.1$  (CBR93), so we have adopted a ‘‘quasi-two-stream’’ approximation to save computing time. In this approximation, it is assumed that stimulated scattering only couples photons in the beam to those traveling antiparallel to the beam direction. This is equivalent to assuming that the scattering cloud has a Thomson depth transverse to the beam direction which is much less than the optical depth along the beam direction, or assuming that only a small portion of the scattering region is illuminated at one time. In any event, the effects that we describe will only be enhanced in a fully three-dimensional treatment.

The source spectrum in all of the simulation runs presented here is

$$\tilde{y}(\tilde{v}) = \tilde{y}_0 \tilde{v}^{3/2} \{1 - \exp(-\tilde{v}^{-11/2})\}, \quad (14)$$

where  $\tilde{y}_0$  is the extrapolation of the high-frequency spectrum to  $\tilde{v} = 1$ . This spectrum has the limiting form

$$\tilde{y}(\tilde{v}) \simeq \tilde{y}_0 \times \begin{cases} \tilde{v}^{3/2} & \tilde{v} \ll 1 \\ \tilde{v}^{-4} & \tilde{v} \gg 1 \end{cases} \quad (15)$$

and is chosen to approximate a steep-spectrum ( $S_\nu \propto \nu^{-3}$ ) synchrotron source which becomes self-absorbed near  $\tilde{v} = 1$ . We note that

$$kT_B / m_e c^2 = \tilde{y}(\tilde{v}) / \tilde{v} \quad (16)$$

is dimensionless and therefore independent of the particular scaling chosen for  $\tilde{y}$  and  $\tilde{v}$ .

### 4. SIMULATION RESULTS

#### 4.1. Reflectivity, Transmittance, and Absorptivity

In Figure 1a we have plotted the fraction of the incident photon number flux which is reflected ( $\mathcal{R}_n$ ), transmitted ( $\mathcal{T}_n$ ), and absorbed ( $\mathcal{A}_n$ ) as a function of the peak  $T_B$  of the source. The scattering slab has a Thomson depth  $\tau_T = 0.2$  and the beam opening angle is  $\theta = 0.1$ . The fraction of the photons that are reflected by spontaneous scattering is  $\sim \tau_T \sim 0.2$ , independent of the incident flux density.

Stimulated scattering increases the fraction of the incident photon number flux which is reflected and/or absorbed by the scattering plasma, with a consequent reduction in the transmitted number of photons, when  $\tau_{BS} \gtrsim 1$ . For the slab parameters used in the run displayed in Figure 1 this occurs at  $kT_B / m_e c^2 \simeq 2500$ , as is seen in the figure. At larger  $T_B$ , the reflectivity saturates at  $\mathcal{R}_n \simeq 0.35$  and the absorptivity begins to rise. This saturation is caused by the back reaction

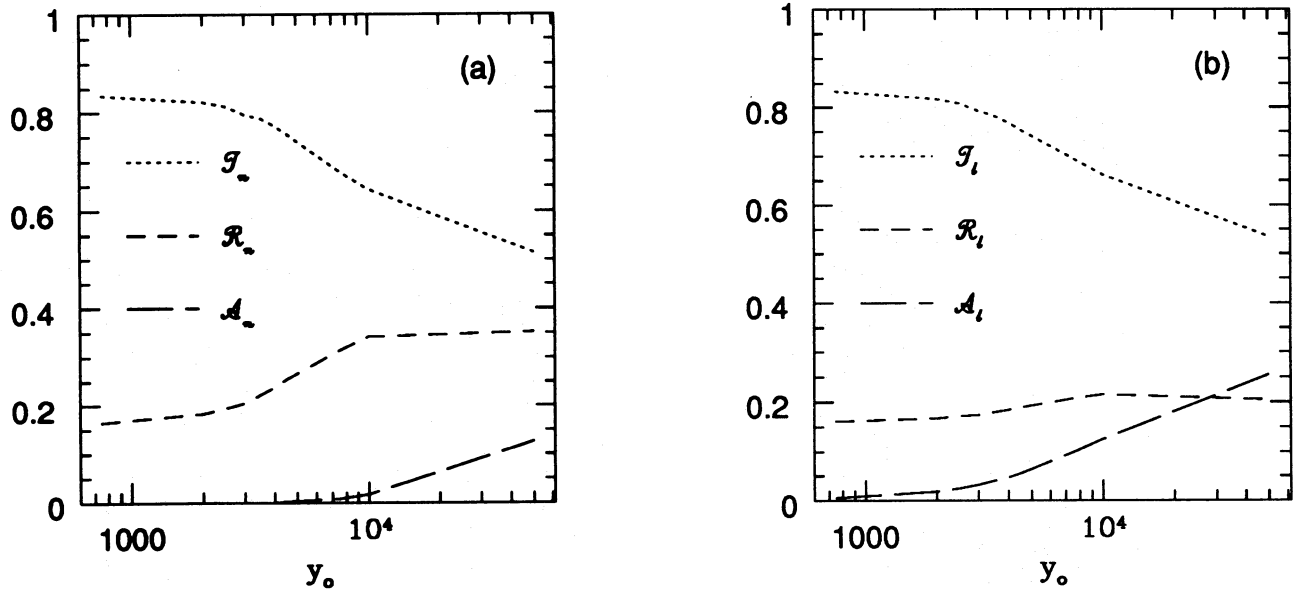


FIG. 1.—The reflectivity ( $\mathcal{R}$ ), transmittance ( $\mathcal{T}$ ), and absorptivity ( $\mathcal{A}$ ) of the plasma as a function of the brightness temperature of the incident radiation. (a) The number fractions; (b) the luminosity fractions.

of the reflected radiation on the beam, and will be discussed in more detail in the next section. We note that, strictly speaking, induced Compton scattering does *not* absorb photons since the process conserves photon number. Rather, it simply moves photons downward in frequency. However, if one observes over a finite range of frequencies (e.g., the reflectivity shown in Fig. 1 is computed by counting up only photons with frequency  $0.01\nu_0 < \nu < 100\nu_0$ ), then one sees an effective absorption as photons are shifted to frequencies below the observed frequency range. Although photons which reach very low frequencies eventually are absorbed by other processes in the plasma such as free-free or synchrotron absorption, the apparent number absorptivity  $\mathcal{A}_n$  in general depends on the range of frequencies being observed.

Stimulated scattering also increases the fraction of the total energy that is reflected ( $\mathcal{R}_l$ ) or absorbed ( $\mathcal{A}_l$ ) by the slab, with a corresponding decrease in the transmittance ( $\mathcal{T}_l$ ). The effects are not as pronounced as for the number flux (see Fig. 1b) because stimulated scattering primarily affects radiation at the low-frequency, low-energy, high brightness temperature end of the spectrum. We also see in Figure 1b that more energy is absorbed than is reflected when the reflectivity saturates. In contrast to the number absorptivity  $\mathcal{A}_n$ , the energy absorptivity  $\mathcal{A}_l$  does represent a real absorption of photon energy since induced Compton scattering transfers energy from photons into the recoil motion of electrons. The quantity  $\mathcal{A}_l$  does depend on the frequency range being observed, but much less so than  $\mathcal{A}_n$  since photons shifted out of the observed frequency range usually carry a negligible amount of energy.

#### 4.2. The Radiation Spectrum

We define the onset of induced Compton backscattering to occur when stimulated scattering has amplified the backscattered intensity by a factor of 2 over the spontaneously scattered level. In § 2 we argued that the backscattered intensity grows exponentially in the early stages of the non-linear evolution. Thus, we expect the onset criterion to be equivalent to  $\tau_T \propto (m_e c^2 / kT_B \theta^2)$ , the  $e$ -folding scale. This

conjecture is confirmed in the simulations, and we find that for a wide range of slab and beam parameters, onset occurs when

$$\tau_{\text{onset}} = \frac{kT_B}{m_e c^2} \tau_T \theta^2 = 1.2, \quad (17)$$

where  $T_B$  is the brightness temperature at the peak of the radiation spectrum. We note that this quantity is linearly dependent upon  $\tau_T$ , in contrast to our definition of  $\tau_{\text{BS}}$  (eq. [10]).

The spectrum of the reflected radiation will be significantly distorted when  $T_B$  exceeds the critical value defined in equation (17). An example of a case in which  $\tau_{\text{onset}} > 1$ , and the reflected spectrum is amplified exponentially, is presented in Figure 2c. In this figure, we have plotted the steady state spectrum for a model with the parameters

$$\tilde{y}_0 = 2000, \quad \tau_T = 0.2, \quad \theta = 0.1. \quad (18)$$

The curves on this plot indicate the spectra of the illuminating ( $y_i$ ), the reflected ( $y_b$ ), and the transmitted ( $y_f$ ) intensities. In Figure 2c, we plot the ratio of the reflected to the transmitted intensity. At frequencies  $\tilde{\nu} \gg 1$ , where  $T_B$  is small and stimulated scattering has little effect upon the spectrum, we see that the ratio is just that which is predicted from spontaneous scattering

$$\tilde{y}_b \simeq \frac{3}{8} \tau_T \theta^2 \tilde{y}_f \simeq 7.5 \times 10^{-4} \tilde{y}_f, \quad (19)$$

in the quasi-two-stream approximation.

At lower frequencies (i.e.,  $\tilde{\nu} \lesssim 1$ ), stimulated scattering dramatically increases the amplitude of the backscattered intensity compared to the level predicted by spontaneous scattering. In cases where there is mild evolution most of the amplification occurs near the turnover, steepening the reflected spectrum and creating a peak in the reflected spectrum at  $\tilde{\nu} \simeq 1$ . Stimulated absorption of the spontaneously scattered radiation results in a sharp cut-off at  $\tilde{\nu} \sim 1$  and a broad absorption feature at  $\tilde{\nu} \gtrsim 1$ . The width of this feature is  $\sim \tilde{\nu}_1 = \tilde{\nu}_0$ , where  $\tilde{\nu}_0 \simeq 1$  and  $\tilde{\nu}_1$  is defined by  $\tau_{\text{BS}}(\tilde{\nu}_1) = 1$ . At frequencies  $\tilde{\nu} \gg 1$  stimulated scattering is no longer

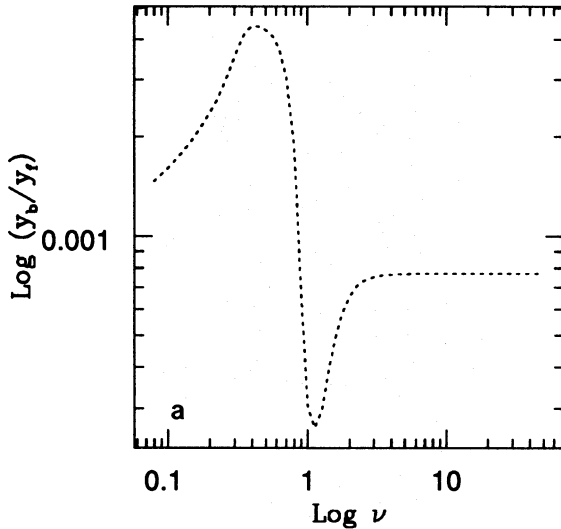


FIG. 2a

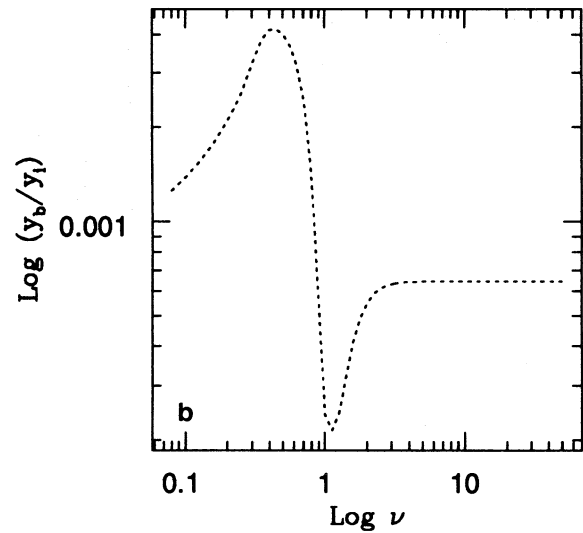


FIG. 2b

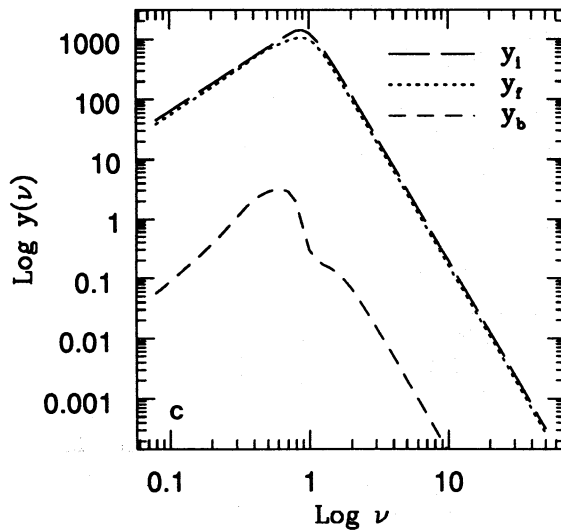


FIG. 2c

FIG. 2.—Plot of (a) the ratio of the backscattered to emergent flux, (b) the ratio of the backscattered flux to the incident flux, (c) the steady state radiation spectrum at the onset of stimulated backscattering. Model parameters are presented in the text.

important and the reflected intensity is just the spontaneously scattered radiation. The transmitted radiation is largely unaffected by stimulated scattering.

Induced Compton scattering saturates when the backscatter optical depth,  $\tau_{BS}$ , becomes large enough. At saturation, the low-frequency spectral indices of both the reflected and transmitted intensities approach the equilibrium value  $\alpha = 1$ , or  $S_\nu \propto \nu$ . The ratio of the reflected to the transmitted intensities also reaches its maximum value

$$\tilde{y}_b \simeq 4\theta^2 \tilde{y}_f \quad (20)$$

at the saturation point, which is independent of frequency. The ratio of the reflected intensity to the *incident* intensity remains a strong function of frequency and is largest at low frequencies. Investigating a range of parameters numerically, we find that saturation occurs when

$$\tau_{BS} = \frac{kT_B}{m_e c^2} \tau_T^2 \theta^2 = 3, \quad (21)$$

accurate to one significant figure.

In Figure 3, we display one example of a saturated spectrum. The run parameters are

$$\tilde{y}_0 = 2 \times 10^5, \quad \tau_T = 0.1, \quad \theta = 0.05, \quad (22)$$

and the quantities plotted are the same as in Figure 2. The low-frequency spectra of both the emergent and backscattered radiation are very close to the equilibrium value of  $\alpha = 1$ , and the ratio of these two intensities is nearly flat. The absorption feature in the reflected spectrum near  $\tilde{\nu} = 1$  is evident, as is the return to the spontaneously scattered spectrum at higher frequencies. In Figure 3b, we plot the ratio of the reflected intensity to the incident intensity.

The brightness temperature at the peak of the transmitted radiation spectrum is set by the criterion

$$\frac{kT_B}{m_e c^2} \tau_T^2 \theta^2 = 1.0 \quad (23)$$

if we define the peak frequency ( $\nu_1$ ) as the frequency at which the actual intensity falls to 80% of the extrapolation of the high-frequency optically thin flux density to  $\nu_1$ . The numerically determined criterion in equation (23) is exactly the same as the order of magnitude estimate (Thompson et al. 1994). The spectral intensity peak does not correspond to the peak in  $T_B$  since  $T_B \propto \tilde{y}/\tilde{\nu} \propto \tilde{\nu}^{-1}$  below  $\tilde{\nu} \sim 1$ . The increase in  $T_B$  at low frequencies due to scattering by a plasma external to the emission region is a general feature of induced Compton scattering (Wilson 1982; CBR93).

The line structure reported by CBR93 is not seen in any of our simulations. We have utilized a new definition of the time step (eq. [13]) which introduces just enough numerical viscosity to damp the “ringing instability” which gives rise to these lines (CBR93). A narrow oscillatory absorption feature is seen near the center of the previously mentioned broad absorption feature. It is not clear whether this is a physical feature related to the ringing instability or merely a numerical artifact. Zel’dovich & Sunyaev (1972) have demonstrated that induced Compton scattering can create oscillating rarefactions such as these when the gradient in the photon spectrum becomes steep. If the narrow feature is real, it is unlikely to be observed in realistic radio spectra because of its oscillatory behavior and the low-frequency resolution of VLBI observations.

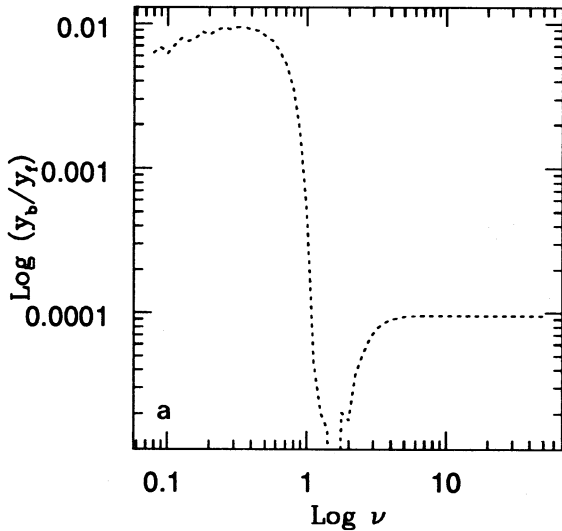


FIG. 3a

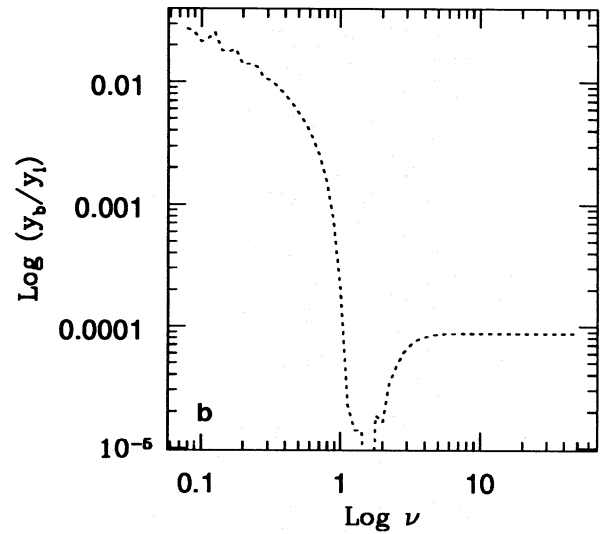


FIG. 3b

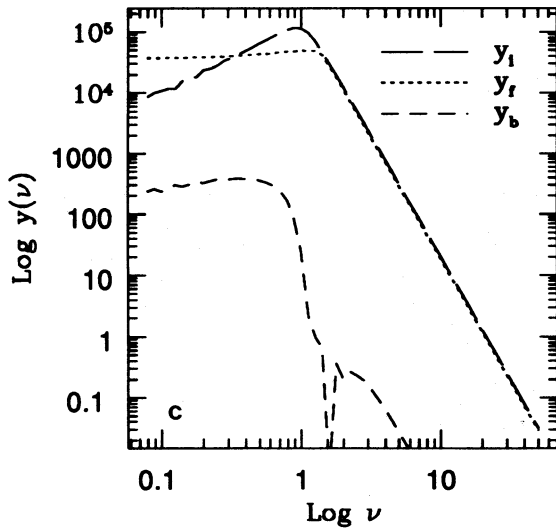


FIG. 3c

FIG. 3.—Plot of (a) the ratio of the backscattered to emergent flux, (b) the ratio of the backscattered flux to the incident flux, and (c) the steady state radiation spectrum at saturation. Note the flat low-frequency spectrum, which is characteristic of saturation. Model parameters are presented in the text.

#### 4.3. Polarization of the Backscattered Radiation

For favorable scattering geometries, Thomson scattering of radiation results in a significant degree of polarization even if the incident radiation is unpolarized. It is therefore worth asking if the induced Compton backscatter process considered here can also give rise to a significant degree of polarization. To answer this question, we turn to the equation for the evolution of a partially polarized, spatially uniform radiation field due to induced Compton scattering (Wilson 1982, see also Coppi 1994):

$$\frac{1}{c} \frac{d}{dt} y_{ij}(\Omega, \omega) = \frac{3}{4\pi} \sigma_T \sum_{k,l,m,n} y_{kl}(\Omega, \omega) \times \int d\Omega' (1 - \cos \phi) M_{ijklmn} \frac{\partial}{\partial \omega} y_{mn}(\Omega', \omega), \quad (24)$$

where

$$M_{ijklmn} = \frac{1}{2} [\delta_{ik}(\epsilon_i \cdot \epsilon_n^*)(\epsilon_j^* \cdot \epsilon_m) + \delta_{jl}(\epsilon_i \cdot \epsilon_n^*)(\epsilon_k^* \cdot \epsilon_m)] \quad (25)$$

and  $\phi$  is the angle between  $\Omega$  and  $\Omega'$ . Here  $y_{ij} \propto \langle E_i E_j^* \rangle$ ,

the expectation value of the product of the components of the electric field along the  $\epsilon_i$  and  $\epsilon_j$  polarization axes.

To analyze the backscattering case, we return to the two-component model of the radiation field. We further simplify the model by neglecting the angular extent of the primary and secondary beams and assume that  $y_p(\Omega) = y_p \delta(\Omega - \Omega_b)$  and  $y_s(\Omega) = y_s \delta(\Omega + \Omega_b)$ , where  $\Omega_b$  is a unit vector in the direction of the beam axis. As in the preceding discussion, the large-amplitude (primary) beam initially evolves very little. Let us treat it as constant and examine the evolution of the secondary component. The kinetic equations for linearly polarized radiation are then

$$\frac{1}{c} \frac{d}{dt} y_{s,0} = \frac{3}{2\pi} \sigma_T y_{s,0} \frac{\partial}{\partial \omega} y_{p,0}, \quad (26)$$

$$\frac{1}{c} \frac{d}{dt} y_{s,1} = \frac{3}{2\pi} \sigma_T y_{s,1} \frac{\partial}{\partial \omega} y_{p,1}, \quad (27)$$

where the subscripts (0, 1) refer to the two orthogonal linear polarization states. These equations have the same form as the kinetic equations for unpolarized radiation, and we expect each polarization state to evolve in the manner previously described. It is obvious that the two polarization states of the backscattered radiation field evolve at the same rate if the primary flux is unpolarized ( $y_{p,0} = y_{p,1}$ ), and therefore no polarization develops in the backscattered flux. This is because the Thomson scattering cross section is front-back symmetric.

Significant polarization of the backscattered flux can form, however, if the primary flux is polarized. From equations (26) and (27), we see that even if the primary beam is only slightly polarized (i.e.,  $y_{p,0} \neq y_{p,1}$ ), induced scattering will exponentially amplify the polarization of the backscattered radiation field. This amplification can occur only if the brightness temperature of at least one of the polarization states satisfies equation (17). In contrast to spontaneous Thomson scattering, the degree of polarization increases strongly with decreasing frequency because the exponential amplification of the backscattered field is strongest at low frequencies (see Fig. 3). In numerical experiments, an initial polarization  $\sim 1\%$  could grow to a polarization  $\sim 50\%$  at low frequencies (e.g., see Coppi 1994). The detection of significant frequency-dependent polarization would be strong evidence that induced scat-

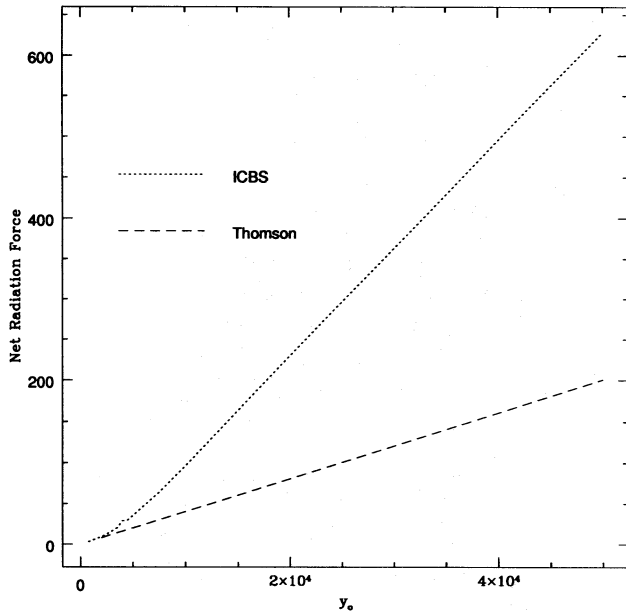


FIG. 4.—Comparison of the net force on a scattering cloud due to Thomson scattering and stimulated (ICBS) scattering.

tering is indeed occurring, particularly if the polarized flux has a spectrum  $S_\nu \propto \nu$ .

4.4. Induced Pressure Gradients and Radiative Acceleration

Stimulated scattering enhances the rate at which momentum is transferred to the scattering electrons and thus enhances the radiation force on the slab. In a steep spectrum source ( $\alpha < -2$ ), most of the momentum is carried by photons near the peak of the brightness temperature distribution. The energy of these photons is efficiently removed by stimulated scattering, leading to a large enhancement in the radiation force. For flatter spectrum sources ( $\alpha > -2$ ), however, most of the momentum is carried by photons at the high-frequency, low brightness temperature end of the spectrum, where stimulated scattering effects are unimportant. The radiation force enhancement in such sources is

thus correspondingly small. The models displayed in this paper are all steep spectrum ( $\alpha = -3$ ) sources.

In Figure 4 we plot the net force (in model units) on the slab caused by stimulated and spontaneous Compton scattering of the incident radiation. The dimensionless model force along the beam direction is calculated by integrating the net rate at which momentum is transported into the slab with the radiation field

$$F_{\text{model}}(\tau) = \int \tilde{y}(\tilde{\nu}, \tau, \Omega)(\Omega \cdot dS)\tilde{\nu} d\tilde{\nu} d\Omega \quad (28)$$

over the surface of the slab,  $S$ . The inclusion of stimulated scattering causes an obvious, but not very dramatic, increase in the net force on the slab. More interesting effects are found when we consider where in the slab the force is deposited.

The model steady-state radiation spectra computed in § 4.2 can be used to calculate the radiation pressure distribution in the slab. The diagonal component of the radiation pressure tensor corresponding to the beam direction is

$$\tilde{P}(\tau) = \int \tilde{y}(\tilde{\nu}, \tau, \Omega)\tilde{\nu} d\tilde{\nu}(\Omega \cdot \hat{n})^2 d\Omega, \quad (29)$$

where  $\hat{n}$  is a unit vector in the direction of the beam. The dimensionless pressure is related to the physical radiation pressure by

$$P(\tau) = \frac{2m_e}{c} \left( \frac{\nu_0}{\tilde{\nu}_0} \right)^3 \tilde{P}(\tau). \quad (30)$$

The remaining components of the pressure tensor are also nonzero, but they make no net contribution to the force on the slab because of the azimuthal symmetry of the scattering processes.

Stimulated scattering slightly increases the radiation pressure at the inner edge of the slab and reduces the pressure at the outer edge. In Figure 5a we have plotted the model radiation pressure for the same parameters as the run

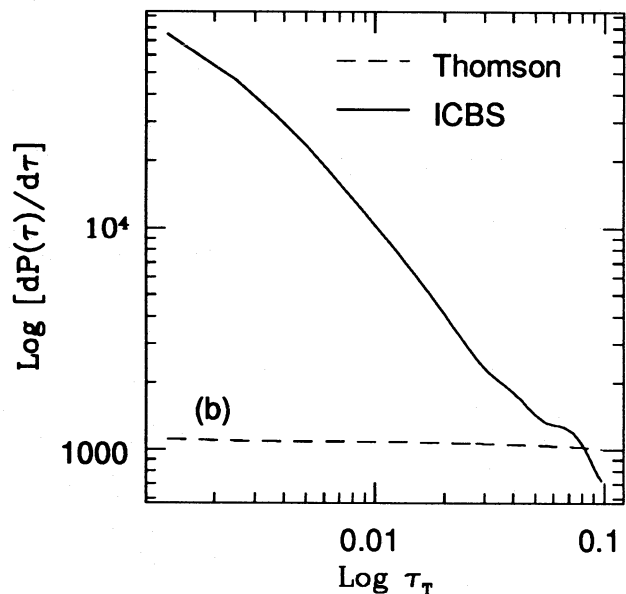
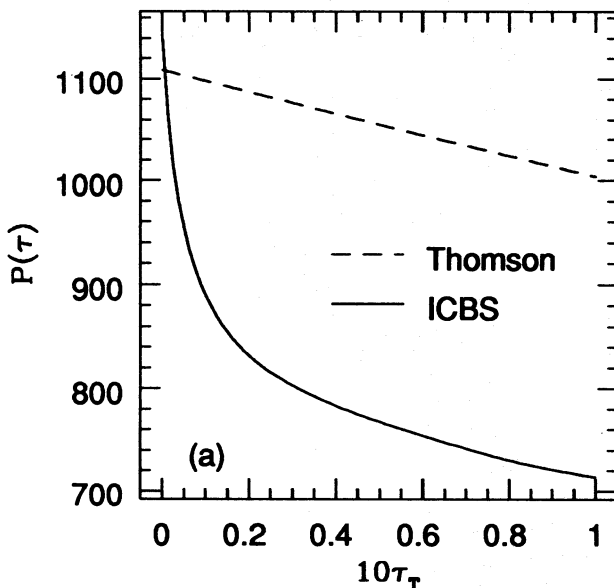


FIG. 5.—Plot of (a) the model radiation pressure through the scattering slab and (b) the pressure gradient for both spontaneous Thomson scattering and induced Compton backscattering (ICBS).

shown in Figure 3. Most of the absorption takes place in the transition region  $\Delta\tau$ , defined by

$$\frac{kT_B}{m_e c^2} (\Delta\tau_T)^2 \theta^2 \simeq 1, \quad (31)$$

which in this case is  $\Delta\tau_T \simeq 0.04$ . When the incident flux is high enough that the steady-state spectrum is saturated,  $\Delta\tau_T \ll \tau_T$ , and the pressure gradient at the inner edge of the slab will be magnified. The model pressure gradient for this set of parameters is plotted in Figure 5b. As expected, the gradient at the inner edge of the slab is magnified by more than an order of magnitude and exceeds the spontaneous scattering value throughout the transition region. Since the momentum lost by the radiation field is transferred directly to the scattering particles, the model pressure gradient can be rewritten as an acceleration along the direction of the beam

$$g_{\text{rad}} = -\frac{2\sigma_T}{c} \left(\frac{m_e}{m_p}\right) \left(\frac{v_0}{\tilde{v}_0}\right)^3 \frac{d\tilde{P}(\tau)}{d\tau}, \quad (32)$$

where  $m_p$  is the mass of the positively charged particle in the plasma.

A useful analytic approximation to  $g_{\text{rad}}$  at the inner edge of the slab can be derived in the limit of a saturated spectrum. In this case the radiation pressure evolves on an optical depth scale,  $T$ , which is several times the scale over which the secondary component evolves. From the simulations, we estimate

$$T \simeq 10 \frac{\tilde{v}_0}{\tilde{y}_0 \theta^2}. \quad (33)$$

The radiation pressure at the inner edge is approximately

$$\tilde{P}_0 \simeq \pi \tilde{y}_0 \tilde{v}_0^2 \theta^2 \quad (34)$$

so that

$$\frac{d\tilde{P}}{d\tau} \sim \frac{\tilde{P}_0}{T} \sim \frac{\pi}{10} \tilde{y}_0^3 \theta^4 \left(\frac{\tilde{v}_0}{\tilde{v}_0}\right)^2, \quad (35)$$

where we have assumed a steep spectrum illuminating source. The radiative acceleration at the inner edge can then be written

$$g_{\text{rad}} \simeq -\frac{\pi}{5} \frac{\sigma_T}{c} \left(\frac{m_e}{m_p}\right) v_0^3 \theta^4 \left(\frac{kT_B}{m_e c^2}\right)^2 \quad (36)$$

using equation (32). Therefore, the acceleration at the inner edge of a slab which is illuminated by a high brightness temperature beam can be enhanced by many orders of magnitude, although the net force on the slab is only slightly enhanced.

## 5. DISCUSSION

### 5.1. Scattering in Radio Pulsar Magnetospheres

The pulsed emission from radio pulsars will be extremely well collimated by the time it reaches the light cylinder radius ( $\theta \sim r_{\text{NS}}/r_L \sim 2 \times 10^{-4}/P$ , where  $r_{\text{NS}}$  is the assumed neutron star radius of 10 km,  $r_L = Pc/2\pi$ , and  $P$  is the pulse period). Thus,  $\tau_T \gtrsim \theta^2$  for very modest values of the Thomson depth of the wind, indicating that stimulated backscattering could play an important role in determining the spectrum of the observed radiation. We note that SK92 calculated the induced Compton scattering depth of a mag-

netized pulsar wind for the case of in-beam scattering, i.e., assuming no photons outside of the beam.

In order to estimate the Thomson depth of a pulsar wind, we adopt the conventional view (Kennel, Fujimura, & Pellat 1979) and assume that the region outside of the pulsar light cylinder can be described as a relativistic spherically symmetric magnetized MHD wind. The MHD wind carries the spin-down luminosity of the pulsar in the form of magnetic fields and relativistic particles. In the MHD approximation, the particles are tied to the field lines and propagate outward at nearly the speed of light. The total spin-down luminosity,  $L_{\text{sd}}$ , can be divided into two components

$$L_{\text{sd}} = L_p + L_B = (1 + \sigma)L_p, \quad (37)$$

where  $L_p$  and  $L_B$  are the energy carried in the particles and the fields, respectively, and

$$\sigma = \frac{B^2}{4\pi\gamma m_p c^2 n_e} \quad (38)$$

is the ratio of the field energy density to the particle energy density. We will also assume that the electrons are cold in the rest frame of the relativistic wind. The Lorentz factor of the wind,  $\gamma$ , can be related to  $\sigma$  by associating it with the velocity of disturbances in an MHD wind,  $\gamma \simeq (1 + \sigma)^{1/2}$  (Ginzburg 1979).

The electron density in the wind can be written in terms of the  $\sigma$  parameter

$$n_e(r) = \frac{L_{\text{sd}}}{(1 + \sigma)^{3/2}} \frac{1}{m_e c^2} \frac{1}{4\pi r^2 c}. \quad (39)$$

The spin-down luminosity of a pulsar is given by

$$L_{\text{sd}} = 4\pi^2 I \frac{\dot{P}}{P^3}, \quad (40)$$

where  $I$  is the moment of inertia of the neutron star and  $\dot{P}$  is the period derivative. Scaling equation (39) to typical pulsar parameters, we find

$$n_e(r) = \frac{4 \times 10^6}{(1 + \sigma)^{3/2}} \left(\frac{r_L}{r}\right)^2 I_{45} \dot{P}_{-15} P^{-5} \text{ cm}^{-3}, \quad (41)$$

where  $I$  is measured in units of  $10^{45} \text{ g cm}^2$ ,  $P$  is measured in seconds, and the period derivative is  $10^{-15}$ .

We will confine our discussion to nonresonant scattering in the magnetized wind because the strong frequency dependence of the resonant scattering cross section significantly complicates the description of stimulated backscattering (for a discussion of resonant scattering see SK92). Even in the nonresonant case, particles are constrained to move along the magnetic field lines. This alters the form of the electron recoil and suppresses nonresonant stimulated scattering until  $r \gtrsim r_* = \gamma^{1/2} r_L$  (SK92). The constraint on the particle motion also implies that only radiation polarized parallel to the magnetic field can be nonresonantly scattered. Therefore, we expect that strong nonresonant stimulated scattering will result in  $\sim 100\%$  polarization of the pulsed radio emission if the field is completely ordered throughout the scattering region, or complete obscuration of the pulse if it is not. Neither of these effects are seen in the integrated pulse profiles and we conclude that stimulated scattering is not occurring in the magnetosphere. We can use this conclusion in conjunction with our numerical cal-

ulation of the backscatter optical depth to set constraints on the content of the wind along the path of the radio emission, if we assume that the bead-on-a-wire scattering cross section is approximately equal to the Thomson scattering cross section at  $r \gtrsim r_*$ .

Induced Compton backscattering is the dominant scattering process when  $\tau_T/\theta'^2 \gtrsim 1$ , where  $\theta' = \gamma\theta$ . Note that this condition must be satisfied in the rest frame of the relativistic wind and primes indicate quantities measured in this frame. Evaluating this ratio at the scattering radius  $r_*$ , we find that stimulated backscattering has a larger effect than in-beam scattering in pulsars with periods

$$P \lesssim 5.4(1 + \sigma)^{-9/8} r_{e,5}^{-1} I_{45}^{1/2} \dot{P}_{-15}^{1/2} \text{ s}, \quad (42)$$

where  $r_{e,5}$  is the radius of the emission region in kilometers. The  $\sigma$  parameter is not well determined and may range from  $10^{-3}$  to  $10^5$  through the magnetosphere. Polar cap models of the multiwavelength emission from the Crab pulsar estimate  $\sigma \sim 10^4$  inside of the light cylinder (Cheng, Ho, & Ruderman 1986), whereas models of the Crab nebula require  $\sigma \sim 10^{-3}$  at much larger radii (Kennel & Coroniti 1984). In the remainder of this discussion, we will assume that  $\sigma \lesssim 10^3$  at the scattering radius. If  $\sigma \gtrsim 10^3$  at the scattering radius, then stimulated backscattering is less important and the description of induced Compton scattering in pulsar winds given by SK92 is the correct one.

Proceeding under the assumption that equation (42) is satisfied, we find that the optical depth of the wind to induced Compton backscattering is

$$\begin{aligned} \tau_{\text{BS}} &= (kT'_B/m_e c^2) \tau_T^2 \theta'^2 \\ &= 6.3 \times 10^{-10} (1 + \sigma)^{-7/2} r_{e,5}^2 T_{B,26} I_{45}^2 \dot{P}_{-15}^2 P^{-10}, \end{aligned} \quad (43)$$

where we have again evaluated this quantity at  $r_*$ . The observed brightness temperature  $T_{B,26}$  is measured in units of  $10^{26}$  K, and we have used the relation

$$T'_B = \frac{T_B}{2\gamma}, \quad (44)$$

which applies in the limit  $\gamma\theta \ll 1$ . Thus, we find that pulsars with periods

$$P \lesssim 0.1(1 + \sigma)^{-7/20} r_{e,5}^{1/5} T_{B,26}^{1/10} I_{45}^{1/5} \dot{P}_{-15}^{1/5} \text{ s} \quad (45)$$

have backscattering optical depths greater than unity. This result is largely insensitive to the wind parameters and  $T_B$  and depends primarily on the very reasonable assumption  $n_e \propto r^{-2}$ . This relation lies nearly coincident to the pulsar "death line"  $\dot{P} \propto P^5$  (Michel 1982), but the highest backscatter optical depths are predicted in the region of the  $P - \dot{P}$  plane which is occupied by all the known pulsars. Induced Compton backscattering in a spherically symmetric MHD wind should obscure the pulsed radio emission from all of these pulsars.

The result suggests that pulsar winds are not spherically symmetric and the observed pulsed emission passes through a region of the magnetosphere which is extremely underdense relative to the predictions of the simple wind model. However, if we assume that only a fraction  $f_w$  of the pulsar spin-down luminosity is directed along the path of the radio emission, then  $f_w \lesssim 10^{-5}$  for  $\tau_{\text{BS}} \lesssim 1$  over the entire distribution of pulsars. A similar value is required to invalidate the assumption that stimulated backscattering is the domi-

nant absorption process in the wind. It would be very surprising to discover that significant regions of the pulsar wind are this rarefied.

A second possibility is that the large pressure gradients created by stimulated backscattering where  $\tau_{\text{BS}} \gtrsim 1$  may drive the scattering particles out of the path of the beam, thereby creating an underdense channel for the pulsed emission. We can use equation (36) to show that

$$g_{\text{rad}} \simeq 2 \times 10^5 \left( \frac{m_e}{m_p} \right) r_{e,5}^4 T_{B,26}^2 \nu_9^3 P^{-4} \text{ cm s}^{-2} \quad (46)$$

at  $r_*$ , where  $\nu_9$  is the frequency in GHz. This can be compared to the gravitational acceleration at  $r_*$ ,  $g \sim 8 \times 10^6 (1 + \sigma)^{-1/2} P^{-2} \text{ cm s}^{-2}$ . Obviously, the radiation pressure will be more important in the faster pulsars. The large pressure gradients must be accompanied by some evolution in the flux density spectrum of the beam, most likely on the leading edge of the pulse. Therefore, evidence for this scenario may be found by studying the pulse spectra as a function of pulse phase and searching for the characteristic  $S_\nu \propto \nu$  induced Compton backscattering spectrum.

## 5.2. Reflection Nebulae in Radio-loud AGNs

The advent of high dynamic range VLBA observations (Wilkinson 1987) may make it possible to image dense clouds of material in the innermost regions of AGNs. Clouds surrounding the central radio source will be illuminated by the high brightness temperature radiation from the source. Stimulated scattering effects can enhance the reflected flux density, perhaps making them visible. The predicted flux is very sensitive to the cloud geometry and distribution around the radio source, so we will only make estimates based on a very simple model.

Let us assume that a cloud of radius  $r_c$  lies at a distance  $R$  from a source of high  $T_B$  radio emission. The source size is  $r_s$ . The minimum cloud column density ( $N_c$ ) for which any enhancement occurs is given by equation (17) as

$$N_c \gtrsim 2 \times 10^{24} \left[ \frac{kT_B}{m_e c^2} \left( \frac{r_s}{R} \right)^2 \right]^{-1} \text{ cm}^{-2}. \quad (47)$$

For comparison, a typical estimate of the column density of a broad line is  $N_c \sim 10^{22} \text{ cm}^{-2}$  (Kwan & Krolik 1981) and the cores of compact radio sources have  $r_s \lesssim 1 \text{ pc}$  (Kellerman & Pauliny-Toth 1981). The reflected spectrum from such a cloud will be strongly peaked at a frequency slightly below the peak frequency of the illuminating flux (see Fig. 2).

The backscattered radiation spectrum will be saturated (eq. [21]) for cloud columns

$$N_c \gtrsim 3 \times 10^{24} \left[ \frac{kT_B}{m_e c^2} \left( \frac{r_s}{R} \right)^2 \right]^{-1/2} \text{ cm}^{-2}. \quad (48)$$

The reflected flux density spectrum will be  $S_\nu \propto \nu$  up to a peak frequency which is slightly less than the peak of the illuminating flux. Above this frequency the flux density drops dramatically due to stimulated absorption catalyzed by the steep spectrum of the incident flux. The expected peak flux from such a cloud is found by using equation (20) to relate the reflected intensity to the intensity of the central source

$$S_c \sim 4 \left( \frac{r_c}{R} \right)^2 S_i, \quad (49)$$

where  $S_i$  is the peak illuminating flux from the compact radio core. If  $r_c \sim 10R$ , the reflected flux will be a few percent of the total observed flux, and a dynamic range of  $\gtrsim 10^2$  will be necessary to detect the reflection nebulae. This is well within the anticipated dynamic range of the VLBA (Wilkinson 1987).

Stimulated backscattering will enhance the initial polarization of the radiation from the central radio source (e.g., Roberts et al. 1990). Following the discussion of § 4.3, we see that the polarization enhancement is largest at low frequencies and declines at higher frequencies. Therefore, we expect reflection nebulae of this sort to exhibit polarization which greatly exceeds that of the central radio source at low frequencies and declines at higher frequencies. Further, the flux density spectrum should be  $S_\nu \propto \nu$  when observed in polarized light.

Free-free absorption will compete with induced Compton scattering in the inner regions of AGNs. The ratio of the free-free optical depth to the induced backscatter depth is

$$\frac{\tau_{\text{ff},\nu}}{\tau_{\text{BS}}} \simeq 0.002 T_7^{-3/2} \nu_9^{-2} T_{B,12}^{-1} r_{\text{pc}}^{-1} \theta^{-2}, \quad (50)$$

where  $T_7 = 10^7$  K is the electron escape temperature from a  $10^8 M_\odot$  black hole,  $r_{\text{pc}}$  is the size of the region in parsecs, and  $\theta$  is the opening angle of the beamed radiation as seen by the scattering cloud. Thus, induced Compton backscattering is more important at higher frequencies and brightness temperatures, but the relative importance of the two processes depends very strongly on the geometry of the scattering clouds.

## 6. CONCLUSIONS

We have performed a quantitative numerical calculation of the steady state radiation spectrum in an electron slab which is illuminated by collimated high brightness temperature radiation. The reflectivity of the slab is enhanced by stimulated backscattering when

$$T_B \gtrsim 7 \times 10^9 \tau_T^{-1} \theta^{-2} \text{ K} \quad (51)$$

at the peak of the incident radiation spectrum. Above this threshold, stimulated backscattering magnifies the amplitude of the reflected flux by a factor  $\propto \exp[(kT_B/m_e c^2) \tau_T \theta^2]$  over the level predicted by purely spontaneous scattering. This leads to a strong peak in the reflected spectrum near the peak of the incident flux density spectrum.

The ratio of the reflected intensity to the transmitted intensity reaches its maximum value of  $4\theta^2$  when the brightness temperature of the illuminating radiation is

$$T_B = 2 \times 10^{10} \tau_T^{-2} \theta^{-2} \text{ K}. \quad (52)$$

This ratio is independent of frequency because stimulated backscattering drives the low-frequency intensity spectrum of both the reflected and transmitted radiation to the equilibrium spectral index of  $\alpha = 1$ . However, the induced Compton absorption of the spontaneously scattered radiation, catalyzed by the steep spectrum beam radiation, results in a sharp cutoff in the reflected intensity at  $\nu \gtrsim \nu_0$ , where  $\nu_0$  is the peak of the spectrum of the illuminating radiation. In contrast, the ratio of the reflected intensity to the *incident* intensity is strongly frequency-dependent over the entire range of frequencies and is much larger at lower frequencies.

ted flux density spectrum is limited to

$$T_B(\nu_1) = 5 \times 10^9 \tau_T^{-2} \theta^{-2} \text{ K}, \quad (53)$$

where  $\nu_1$  is the frequency at the peak. Below this frequency, the scattering material becomes optically thick to induced Compton backscattering and the flux density approaches  $S_\nu \propto \nu$ . This result is, surprisingly, in complete agreement with the simple order-of-magnitude estimate used to calculate the induced Compton backscattering optical depth of the eclipsing material in eclipsing millisecond pulsars (Thompson et al. 1994).

The polarization of the reflected radiation can be enhanced by induced Compton backscattering over the level predicted by spontaneous Thomson scattering if  $T_B \gtrsim 7 \times 10^9 \tau_T^{-1} \theta^{-2}$  K in at least one of the polarization states of the radiation. However, if the incident flux is unpolarized, there will be no net change in the polarization of the backscattered flux. The enhancement in the polarization is greatest at low frequencies (numerical experiments suggest that an initial polarization of 1% can be increased to  $\sim 50\%$ ) and declines as the observing frequency increases.

Enhanced radiation pressure gradients are formed by the rapid absorption of photon momentum at the inner edge of the scattering slab. In steep spectrum sources ( $\alpha \lesssim -2$ ) the pressure gradient increases  $\propto T_B^2$  after the stimulated backscattering saturates. Thus, induced Compton backscattering can greatly enhance the radiation pressure force on the scattering plasma. In flatter spectrum sources most of the radiation energy density is at higher frequencies, where the brightness temperatures are lower and stimulated scattering has little effect.

Induced Compton backscattering of the high brightness temperature radiation from pulsars makes this radiation a sensitive probe of the pulsar environment. If we assume that the spin-down luminosity of radio pulsars is carried away in a spherically symmetric relativistic MHD wind which is not completely magnetically dominated (i.e.,  $\sigma \ll 10^4$ ), stimulated scattering would obscure the radio emission from all pulsars with  $P \lesssim 0.1 \dot{P}_{15}^{1/5}$  s. This result implies that the region of the wind through which the pulsed emission propagates must be underdense by a factor of  $\sim 10^{-5}$  relative to the predictions of the simplest model. The large pressure gradients formed by induced scattering may be able to accelerate the scattering material out of the path of the beam, clearing a channel for the radio emission to pass through.

High dynamic range observations using the VLBA (Wilkinson 1987) may make it possible to resolve radio-frequency “reflection nebulae” in the innermost regions of radio-loud AGNs. Stimulated backscattering can enhance the reflected flux density, making these objects observable by instruments with a dynamic range of  $\gtrsim 10^2$ . In addition, the radio emission from the reflection nebulae will be strongly polarized if the illuminating radiation has any net polarization. Thus, radio reflection nebulae in AGNs should be characterized by strong low-frequency polarization, decreasing at higher frequencies, and a flux density spectrum in polarized light of  $S_\nu \propto \nu$ .

We would like to thank Julian Krolik for providing the impetus to start this work and both he and Roger Blandford for continuing conversations. M. W. S. received support for this work from NASA grants NAGW-3129, 1583, and NAG 5-2925; and NSF grant AST 93-15133. P. S. C. received support from a GRO Fellowship and NASA

## REFERENCES

- Cheng, K. S., Ho, C., & Ruderman, M. 1986, *ApJ*, 300, 500  
 Coppi, P. S. 1995, in preparation  
 Coppi, P. S., Blandford, R. D., & Rees, M. J. 1993, *MNRAS*, 262, 603 (CBR93)  
 Ginzburg, V. L. 1979, *Theoretical Physics and Astrophysics* (New York: Pergamon)  
 Gol'din, V. Y., Sunyaev, R. A., & Chetverushkin, B. N. 1975, *Soviet Phys.—JETP Lett.*, 41, 18  
 Kellerman, K. I., Pauliny-Töth I. I. K. 1981, *ARA&A*, 19, 373  
 Kennel, C. F., & Coroniti, F. V. 1984, *ApJ*, 283, 694  
 Kennel, C. F., Fujimura, F. S., & Pellat, R. 1979, *Space Sci. Rev.*, 24, 407  
 Kompaneets, A. S. 1957, *Soviet Phys.—JETP Lett.*, 4, 730  
 Kwan, J., & Krolik, J. H. 1981, *ApJ*, 250, 478  
 Levich, E. V. 1972, *Soviet Phys.—JETP Lett.*, 34, 59  
 Lyne, A. G., & Graham-Smith, F. 1990, *Pulsar Astronomy* (New York: Cambridge Univ. Press)  
 Michel, F. C. 1982, *Rev. Mod. Phys.*, 54, 1  
 Montes, C. 1977, *ApJ*, 216, 329  
 Peyraud, J. 1968a, *J. de Physique*, 29, 88  
 Peyraud, J. 1968b, *J. de Physique*, 29, 306  
 ———. 1968c, *J. de Physique*, 29, 872  
 Roberts, D. H., Kollgaard, R. I., Brown, L. F., Gabuzda, D. C., & Wardle, J. F. 1990, *ApJ*, 360, 408  
 Sincell, M. W., & Krolik J. H. 1992, *ApJ*, 395, 555 (SK92)  
 ———. 1994, *ApJ*, 430, 550  
 Sunyaev, R. A. 1971, *Soviet Astron.—AJ*, 15, 190  
 Thompson, A. C., Blandford, R. D., Evans, C. R., & Phinney, E. S. 1994, *ApJ*, 422, 304  
 Weyman, R. 1965, *Phys. Fluids*, 8, 2112  
 Wilkinson, P. N. 1987, in *Superluminal Radio Sources*, ed. J. A. Zensus & T. J. Pearson (Cambridge: Cambridge Univ. Press), 211  
 Wilson, D. B. 1982, *MNRAS*, 200, 881  
 Wilson, D. B., & Rees, M. J. 1978, *MNRAS*, 185, 297  
 Zel'dovich, Ya. B., & Levich, E. V. 1969, *Soviet Phys.—JETP Lett.*, 28, 1287  
 Zel'dovich, Ya. B., & Sunyaev, R. A. 1972, *Soviet Phys.—JETP Lett.*, 35, 81  
 ———. 1976, *Soviet Phys.—JETP Lett.*, 41, 391